

Visions of *ep* physics

B. Foster^{1,2}

¹ H.H. Wills Physics Laboratory, University of Bristol, Tyndall Avenue, Bristol, BS8 1TL, U.K.

e-mail: b.foster@bris.ac.uk

² DESY, Notkestrasse 85, 22607 Hamburg, Germany.

Received:

Abstract. The subject of lepton-hadron scattering is discussed from its earliest beginnings, concentrating on what we have learnt from the HERA electron-proton storage ring. A brief selection of the HERA I results most relevant to LHC are discussed. The HERA and ZEUS upgrades are outlined, together with the HERA II physics programme. The impact of HERA results on LHC is discussed, in particular in the areas of luminosity measurement, background estimates and possible signatures of new physics. Finally, possible future developments in lepton-proton physics beyond HERA II are discussed.

PACS: not given

1 Introduction

The foundations of the Standard Model consist of a small number of deep theoretical insights based on key experimental observations. Undoubtedly, the quark-parton model and the deep inelastic scattering (DIS) experiments begun at SLAC in the late 1960s are part of these key foundations. Of course, the scattering of energetic “simple” particles from an unknown target to elucidate its structure is an experimental technique with a long and distinguished history. One of the earliest, and perhaps the most famous, is the scattering of alpha particles from a thin gold foil carried out by Geiger and Marsden in Manchester in 1909, which led to the concept of the nuclear atom [1, 2].

In this talk, I will briefly summarise the current status of *ep* physics, concentrating on our knowledge of the proton structure, which, over the majority of the currently explored phase space, comes primarily from HERA results. I will then outline the HERA-II programme and how the ZEUS and H1 experiments have been modified to take advantage of the large increase in luminosity. The main physics aims of the HERA-II programme are outlined. I then discuss the importance and relevance of the HERA-I and HERA-II output to the physics programme of LHC. I conclude with a summary of possible future facilities for *ep* physics and a perspective on the future of this field.

2 Current status of *ep* physics and HERA-I results

With the advent of the HERA electron-proton collider, the explorable phase space in the kinematic invariants Q^2 (the virtuality of the exchanged virtual

photon) and x (the fractional momentum of the parton involved in the scattering) has increased by approximately three orders of magnitude in each variable compared to what was available at earlier fixed-target experiments (see figure 1). This extension in kinematic range has opened up qualitatively new fields of study, both at high and low Q^2 .

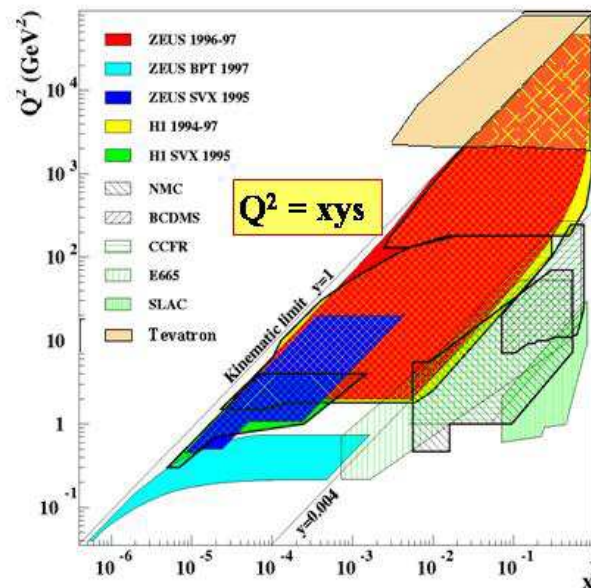


Fig. 1. The kinematic plane in x and Q^2 for experiments probing the parton distribution of the proton. The regions explored by each experiment are shown in a variety of shadings as shown in the legend. Hadron-hadron collisions are also able to measure the proton structure, predominantly at high x and high Q^2 .

2.1 The proton structure function

Undoubtedly the most important observation of the SLAC DIS experiments was that of scaling, as illustrated in figure 2. This shows the νW_2 structure function (nowadays known as F_2) at $\omega (= x^{-1}) = 4$ as a function of Q^2 . The remarkable lack of variation of νW_2 with Q^2 is apparent; it was this that led directly to the postulation by Feynman of the parton model. The interpretation of these data, in retrospect, seems straight-forward. Since Q^2 is approximately proportional to the scattering angle of the electron and the structure function is proportional to the scattering cross section, the flatness corresponds to the production of an excess of particles at large angle compared to that expected from the rapid

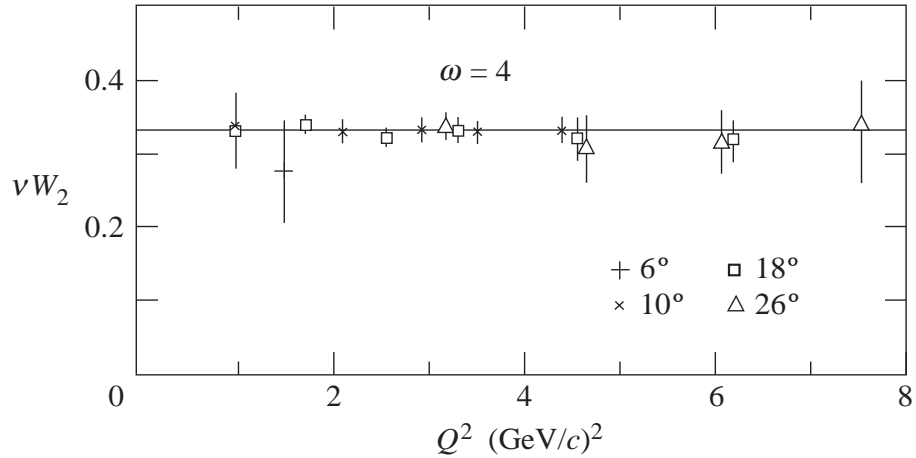


Fig. 2. The νW_2 structure function at $\omega = 1/x = 4$ as a function of Q^2 as measured by the SLAC-MITgroup[3]. Data taken at four different scattering angles are shown. All data is consistent with being independent of Q^2 .

fall off from the form factor of an extended object. The solution is exactly the same as that which presented itself to Rutherford - the incident particle scatters not from an extended “fuzzy” object, the atom, but from point-like scattering centres situated inside it. In his case this was the nucleus; in the case of the SLAC experiment, the point-like scatterers were the quarks.

That this scaling is still a feature of today’s deep inelastic experiments is illustrated by figure 3. In modern terminology, the deep inelastic double-differential neutral current cross section is expressed in terms of structure functions as

$$\frac{d^2\sigma}{dx dQ^2} = \frac{2\pi\alpha^2}{xQ^4} [Y_+ \cdot F_2(x, Q^2) - y^2 F_L(x, Q^2) \pm Y_- \cdot xF_3(x, Q^2)], \quad (1)$$

where the \pm before xF_3 is taken as positive for electron scattering and negative for positron scattering and Y_{\pm} are kinematic factors given by

$$Y_{\pm} = 1 \pm (1 - y)^2, \quad (2)$$

where y is the inelasticity of the interaction. This can be expressed in terms of the other invariants as

$$y = \frac{Q^2}{sx} \quad (3)$$

where s is the squared centre-of-mass energy of the ep system. The F_2 structure function can be expressed, in the “DIS scheme” in a particularly simple way as

$$F_2(x, Q^2) = \sum_{i=u,d,s,c,b} A_i(Q^2) [xq_i(x, Q^2) + x\bar{q}_i(x, Q^2)] \quad (4)$$

The parton distributions $q_i(x, Q^2)$ and $\bar{q}_i(x, Q^2)$ refer to quarks and antiquarks of type i . For $Q^2 \ll M_Z^2$, where M_Z is the mass of the Z^0 boson, the quantities $A_i(Q^2)$ are given by the square of the electric charge of quark or antiquark i .

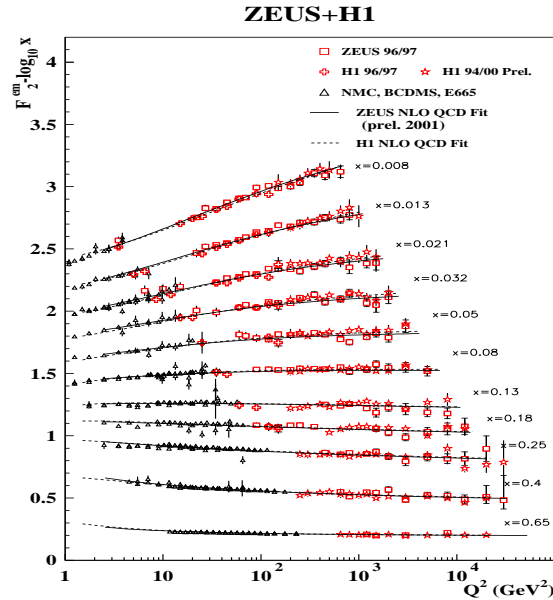


Fig. 3. The F_2 structure function as measured by the H1 and ZEUS experiments for bins at high x as a function of Q^2 . The bins centred around $x = 0.25$ are where scaling was originally observed in the SLAC experiments. Clear scaling violation is observed in the HERA data outside this region, particularly at low x .

The region around $x = 0.25$, in which scaling was observed at SLAC, can be seen in figure 3. Despite the fact that the data [4, 5, 6] now extend over four orders of magnitude in Q^2 , approximate scaling is still observed. However, if one examines the data over the much wider range of x available to the HERA experiments, it is clear that scaling is badly violated at low x . This rapid rise of the structure function at low x (see figure 4) can be attributed to gluon emission and the subsequent production of virtual quark-antiquark pairs, which can in their turn radiate gluons, producing a “sea” of partons at lower and lower x . Thus, the precise measurement of the proton structure at low x at HERA is very sensitive both to the details of the evolution in QCD of this shower of partons and to the value of the strong coupling constant, α_s .

The sensitivity of the evolution of F_2 to the value of α_s has been exploited by both ZEUS and H1. Each experiment has made a global QCD fit to its own data plus some or all of the fixed-target DIS data. There is reasonably good agreement between the experiments, although work still continues on understanding the differing treatments of the errors in the two experiments. The results are shown in figure 5.

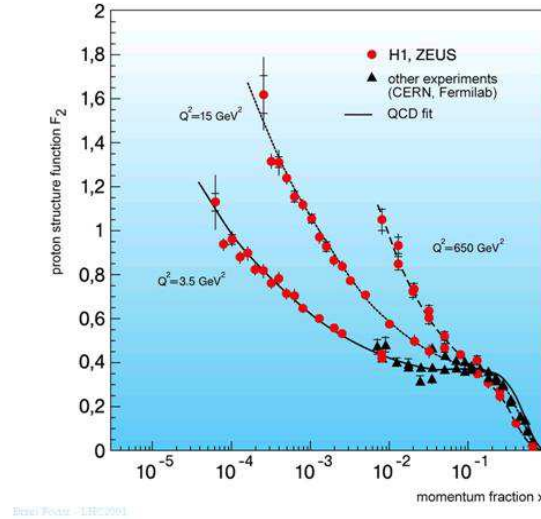


Fig. 4. H1 and ZEUS data on the F_2 structure function shown in three bins of Q^2 as a function of x . The steep rise of the structure function at low x is clearly apparent. The HERA data are now as accurate as the fixed-target data and match onto it well.

Another output of the fit is a value of α_s ; the results from the two experiments are shown in figure 6, labelled as “NLO-QCD fit”. Also shown are a variety of other, high-precision, measurements of α_s that can be made at HERA using a variety of techniques. These include classic methods such as the rate of dijet + proton-remnant production compared to that of single jet plus remnant, the subjet-multiplicity evolution inside jets and the shape of jets. Many of these give excellent precision, comparable to the world average. The dominant uncertainty is usually theoretical and arises from the lack of next-to-next-to-leading-order predictions.

The structure-function data are not only sensitive to QCD effects. The publication of the ZEUS “BPT” data [7] gives access to very low Q^2 and x regimes. As shown by figure 7, although QCD gives a good fit to the data down to $Q^2 \sim 1$ GeV², below that it is necessary to use a Regge-based fit of the form

$$F_2(x, Q^2) = \left(\frac{Q^2}{4\pi^2\alpha} \right) \left(\frac{M_0^2}{M_0^2 + Q^2} \right) \left(A_{\text{R}} \left(\frac{Q^2}{x} \right)^{\alpha_{\text{R}} - 1} + A_{\text{P}} \left(\frac{Q^2}{x} \right)^{\alpha_{\text{P}} - 1} \right), \quad (5)$$

where A_{R} , A_{P} and M_0 are constants and α_{R} and α_{P} are the Reggeon and Pomeron intercepts, respectively. Regge theory is expected to apply at asymp-

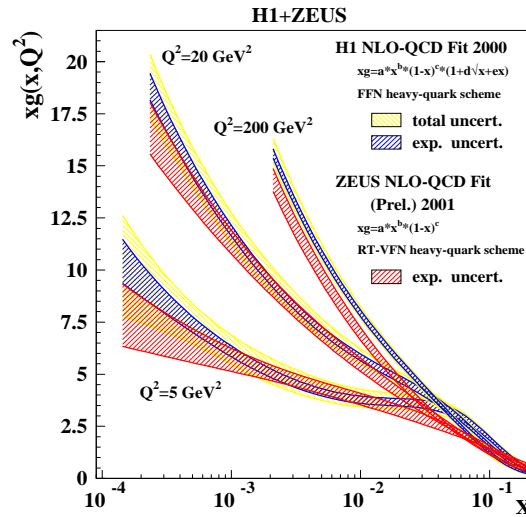


Fig. 5. The gluon density in the proton as measured by ZEUS (red shaded band) and H1 [5] (yellow and blue shaded bands) as a function of x in three bins of Q^2 . The functional form used by the two collaborations in the gluon fit is shown in the legend.

otic energies. The appropriate energy here is W , the centre-of-mass energy of the virtual photon-proton system, which can be expressed in terms of the other invariants as

$$W^2 = Q^2 \frac{1-x}{x}. \quad (6)$$

Since, at low x , $W^2 \sim 1/x$, it would be expected that Regge fits would be applicable at very low x and Q^2 .

Figure 8 shows the ZEUS BPT data, together with both ZEUS and H1 F_2 data, in bins of constant y as a function of $\ln Q^2$. For $Q^2 \gtrsim 1 \text{ GeV}^2$, the data are roughly independent of Q^2 , whereas at lower Q^2 they fall rapidly, approaching the Q^{-2} dependence that would be expected in the limit $Q^2 \rightarrow 0$ from conservation of the electromagnetic current.

The combination of the BPT data and the latest F_2 data means that ZEUS now has precise data over a remarkable six orders of magnitude in x and Q^2 . These data are shown in x bins as a function of $\ln Q^2$ in figure 9, together with fixed target data from NMC and E665, which extends the range in the direction of medium x and Q^2 .

The availability of this very wide range of precise data makes possible qualitatively new investigations of models that describe F_2 . Since the logarithmic derivative of F_2 is directly proportional to the gluon density in leading-order QCD, which in turn is the dominant parton density at small x , its behaviour as a function of both x and Q^2 is important. The solid curves on the figure

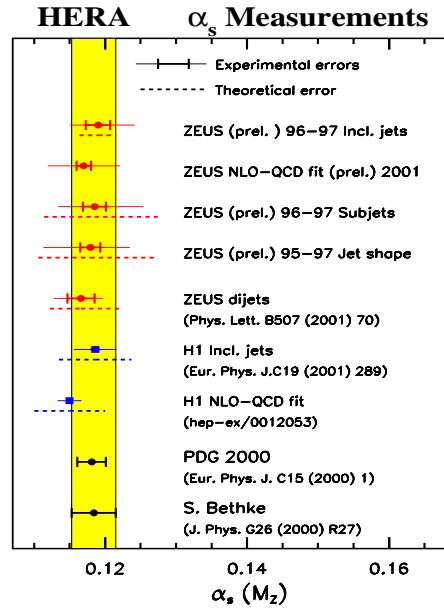


Fig. 6. Values of the strong coupling constant as determined at HERA. Each different measurement is displaced vertically for ease of visibility; each value arises from a different method as briefly indicated in the legend. The reference for published results is shown below the method label. The world average as calculated by the particle data group and by Bethke are shown at the bottom of the figure.

correspond to fits to a polynomial in $\ln Q^2$ of the form

$$F_2 = A(x) + B(x) (\log_{10} Q^2) + C(x) (\log_{10} Q^2)^2, \quad (7)$$

which gives a good fit to the data through the entire kinematic range. The dotted lines on figure 9 are lines of constant W . The curious ‘bulging’ shape of these contours in the small- x region immediately implies that something interesting is going on there. Indeed, simple inspection of figure 9 shows that the slope of F_2 at constant W begins flat in the scaling region, increases markedly as the gluon grows and drives the evolution of F_2 and then flattens off again at the lowest x .

Figure 10 shows the logarithmic derivative evaluated at (x, Q^2) points along the contours of fixed W shown on figure 9 according to the derivative of equation 7, *viz.*:

$$\frac{\partial F_2}{\partial \log_{10} Q^2} = B(x) + 2C(x) \log_{10} Q^2, \quad (8)$$

where the data are plotted separately as functions of $\ln Q^2$ and $\ln x$. The turnover in the derivatives in all W bins is marked. Within the framework of pQCD,

ZEUS+H1 1994–1997

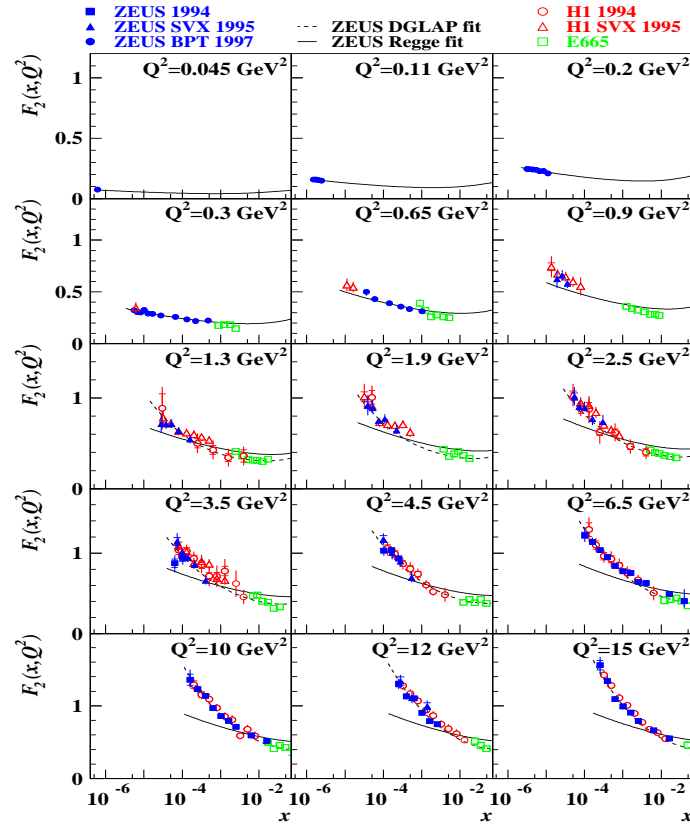


Fig. 7. ZEUS BPT data on F_2 in bins of Q^2 as a function of x . Also shown are earlier ZEUS data as well as data from H1 and E665. The solid line shows the results of the “ZEUS Regge fit to the form of equation 5, while the dotted line shows the result of the ZEUS NLO QCD fit.

the interpretation of such an effect is that the growth of the gluon density at low x is tamed as Q^2 and x fall. Such an effect is by no means necessarily an indication of deviations from the standard DGLAP [8, 9, 10, 11] evolution. Nevertheless, such a fall in the gluon density as x falls is a natural consequence of parton saturation or shadowing. These effects can be naturally discussed in “dipole models” [12], which often explicitly take into account parton-saturation effects. In such models, the “standard” picture of deep inelastic scattering in the infinite-momentum frame of the proton is replaced by an equivalent picture produced by a Lorentz boost into the proton rest frame. In this frame, the virtual photon undergoes time dilation and develops structure far downstream of the interaction with the proton. The dominant configurations of this structure are $q\bar{q}$ and $q\bar{q}g$ Fock states, which interact with the proton as a colour dipole. The

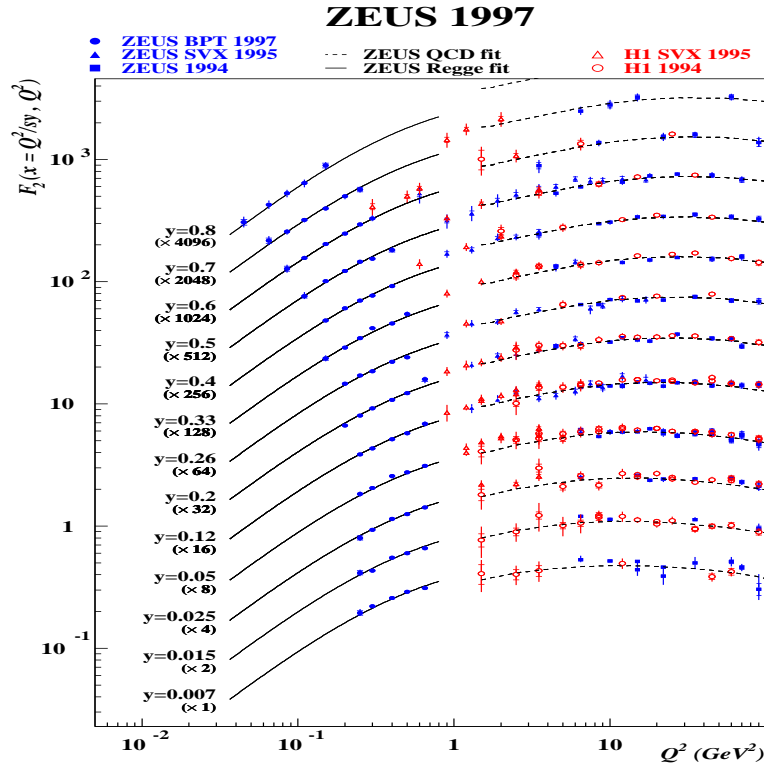


Fig. 8. ZEUS BPT data on F_2 in bins of y as a function of Q^2 . Also shown are earlier ZEUS data as well as data from H1. The solid line shows the results of the “ZEUS Regge fit to the form of equation 5, while the dotted line shows the result of the ZEUS NLO QCD fit.

higher the Q^2 of the interaction, the smaller the transverse size of the dipole. For small x , the deep inelastic process can be considered semi-classically as the coherent interaction of the dipole with the stationary colour field of the proton a long time after the formation of the dipole.

One of the most attractive features of such models is the rather natural way in which they can lead to a unified description of diffraction and deep inelastic scattering. Diffractive DIS is a subset of fully inclusive DIS characterised by a hard interaction between the proton and the exchanged virtual photon that nevertheless leaves the proton intact. The fully inclusive structure functions sum over all possible exchanges between the dipole and the proton, dominantly one- and two-gluon exchange in a colour octet, whereas diffraction is produced by the exchange of two gluons in a colour-singlet state. This deep connection between these two processes leads to non-trivial predictions [13, 14] which do indeed seem to be at least qualitatively in agreement with the data. This is illustrated in figure 11. This figure is surprising for several reasons. It demonstrates that the diffractive cross section has the same W dependence as the total cross section.

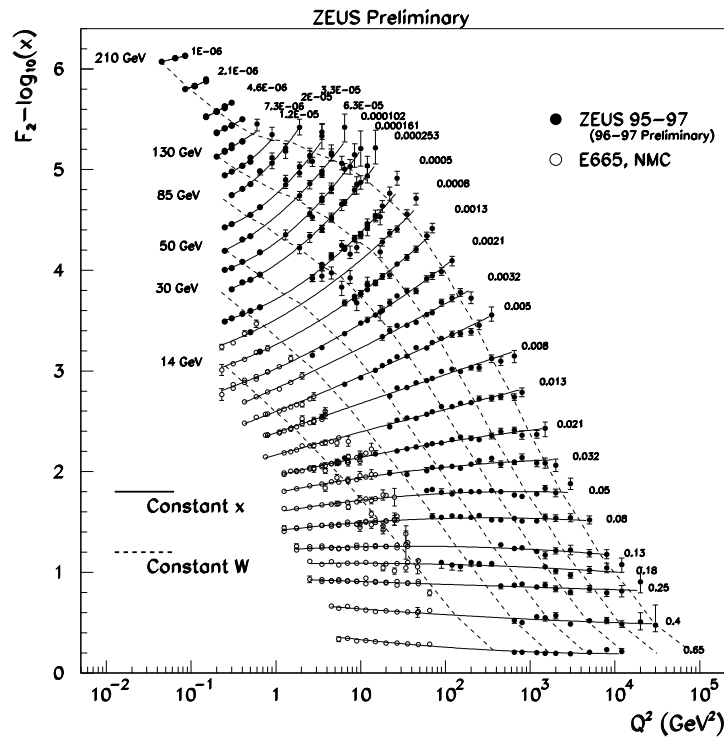


Fig. 9. Compilation of ZEUS F_2 data in x bins as a function of Q^2 . Each x bin is shifted by an additive constant for ease of visibility. Data from NMC and E665 are also shown. The dotted lines show lines of constant W , while the solid lines are fits to the form of equation 7.

To the extent to which the diffractive cross section can be related to the elastic cross section, one would have expected from the Optical Theorem that the ratio would have a power-law dependence on W , as indeed would also be expected from Regge theory via the exchange of a Pomeron. A strong W ($\sim 1/x$) dependence is also expected in QCD models, since the total cross section is dominated by single-gluon exchange, whereas diffraction is dominated by two-gluon exchange. The other surprise is the fact that the GBW model gives a rather good qualitative representation of the data. The behaviour of this ratio as $Q^2 \rightarrow 0$ is also likely to be of great interest. In this talk, however, there is only time to scratch the surface of these interesting low- x and diffractive phenomena, which contain a great deal of information touching on the very challenging problem of confinement in QCD.

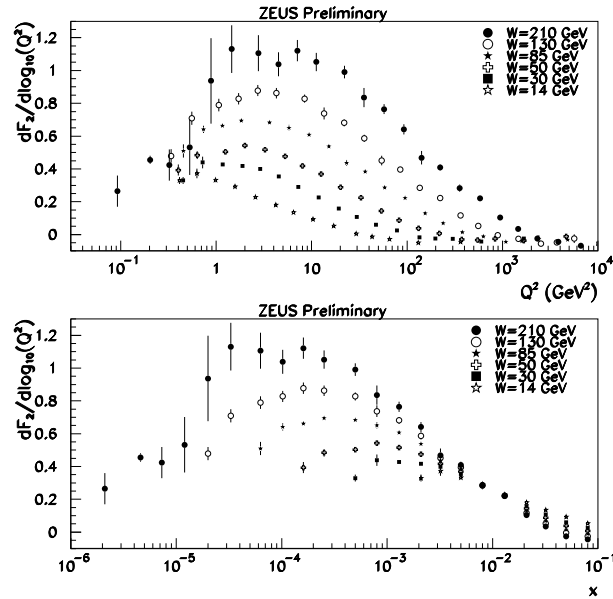


Fig. 10. The logarithmic derivative of the ZEUS F_2 data in six bins of W , plotted as a function of Q^2 and x .

2.2 High- Q^2 phenomena

HERA provides an unique opportunity to study the electroweak interaction at Q^2 sufficiently high that the charged and neutral currents are of similar strength. Figure 12 shows the differential cross-sections for the charged and neutral currents as a function of Q^2 from H1 and ZEUS. It can be seen that, for e^-p interactions, these two processes become of equal strength at $Q^2 \sim M_Z^2 \sim 10^4 \text{ GeV}^2$. For e^+p interactions, the charged current cross-section approaches the neutral current cross-section, but remains below it. The features of this plot can be explained by inspection of equation 1, together with 9 and 10 below:

$$\left. \frac{d^2\sigma}{dx dQ^2} \right|_{e^-}^{CC} = \frac{G_F^2}{2\pi} \left(\frac{M_W^2}{M_W^2 + Q^2} \right)^2 \cdot 2x \{ u(x) + c(x) + (1-y)^2 (\bar{d}(x) + \bar{s}(x)) \} \quad (9)$$

$$\left. \frac{d^2\sigma}{dx dQ^2} \right|_{e^+}^{CC} = \frac{G_F^2}{2\pi} \left(\frac{M_W^2}{M_W^2 + Q^2} \right)^2 \cdot 2x \{ \bar{u}(x) + \bar{c}(x) + (1-y)^2 (d(x) + s(x)) \} \quad (10)$$

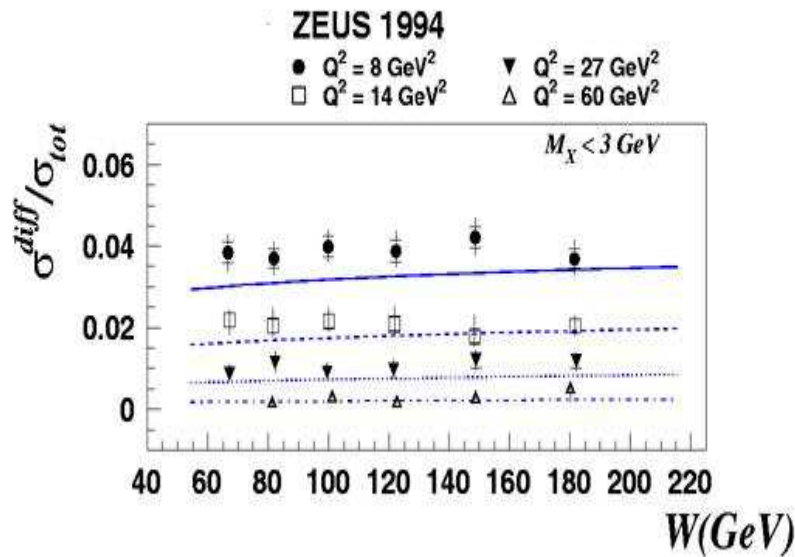


Fig. 11. The ratio of the diffractive to total cross section in four Q^2 bins as a function of W . The curves show the predictions from the Golec-Biernat & Wusthoff model.

For the charged current case, the smaller size of the e^+p cross-section compared to e^-p is related to the fact that, at high Q^2 , equation 3 implies that both $x, y \rightarrow 1$. There are two main contributory factors to the cross-section difference that flow from this. First, there are twice as many u valence quarks inside the proton that can couple to W^- as d quarks that can couple to W^+ . Secondly, the $(1-y)^2$ terms in equations 9 and 10, which arise from the $V-A$ helicity structure of the charged weak current, imply that the valence-quark contribution, which is dominant at high Q^2 , is suppressed for the positron case but not for electrons.

The difference between the electron and positron neutral current cross sections shown in equation 1 allows the determination of the parity-violating structure function xF_3 by taking the difference of the cross sections. The results [15] are shown in figure 13. This is clearly a very difficult measurement since it requires the subtraction of two quantities that are almost equal. The measurement is dominated by statistical errors and particularly by the fact that the electron data sample that has so far been obtained at HERA is much smaller than that for positrons.

The high- Q^2 regime is also interesting since possible new states from electron-quark fusion (e.g. leptoquarks) have masses given by $M^2 \sim sx$ and since the sensitivity to the effects of new currents is maximised. An example of the sensitivity that can be obtained at HERA is shown in figure 14, which shows the mass against coupling limits for two varieties of scalar leptoquark. Both H1 and

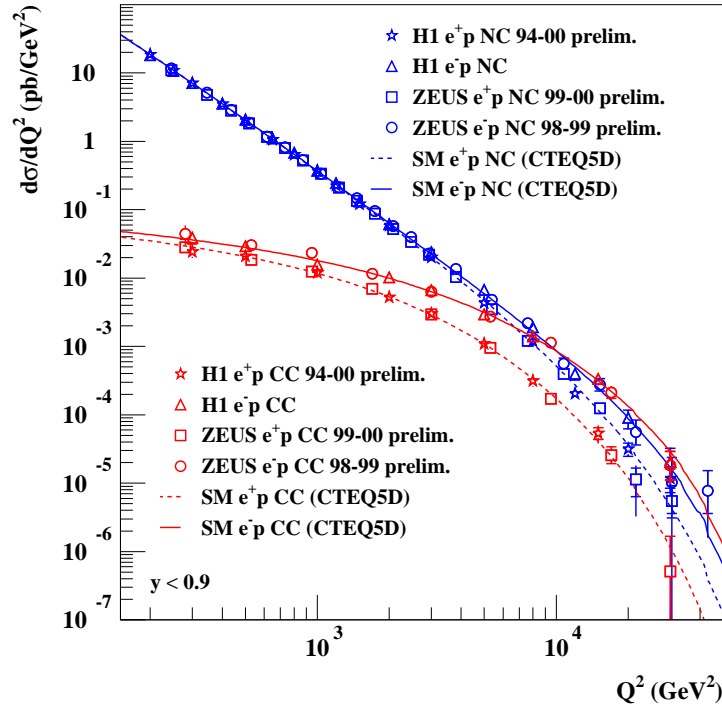


Fig. 12. Charged and neutral current differential cross sections for e^\pm scattering as a function of Q^2 from H1 and ZEUS.

ZEUS have comparable limits for a whole range of such states with differing quantum numbers. It can be seen from figure 14, and it is generally the case, that for some states, in particular in R -parity violating supersymmetry models or leptoquarks, HERA has higher sensitivity than either LEP or the Tevatron.

As well as stringent limits on new phenomena, the HERA data also show intriguing features which may be signatures for new physics. The H1 collaboration has observed a class of events that have isolated charged leptons with large missing transverse momentum. Figure 15 shows the distribution of the transverse momentum of the hadronic system, p_T^X , against its transverse mass separately for electrons (or positrons) and muons in such events. Also shown are the expectations from the Standard Model background, which is dominated by single W production.

It can be seen that the distribution of the events is rather different to the Standard Model expectation. Furthermore, H1 sees an excess of such events. For the transverse mass of the hadronic system greater than 25 GeV, H1 sees four electron and six muon events, compared to Standard Model expectations of 1.3

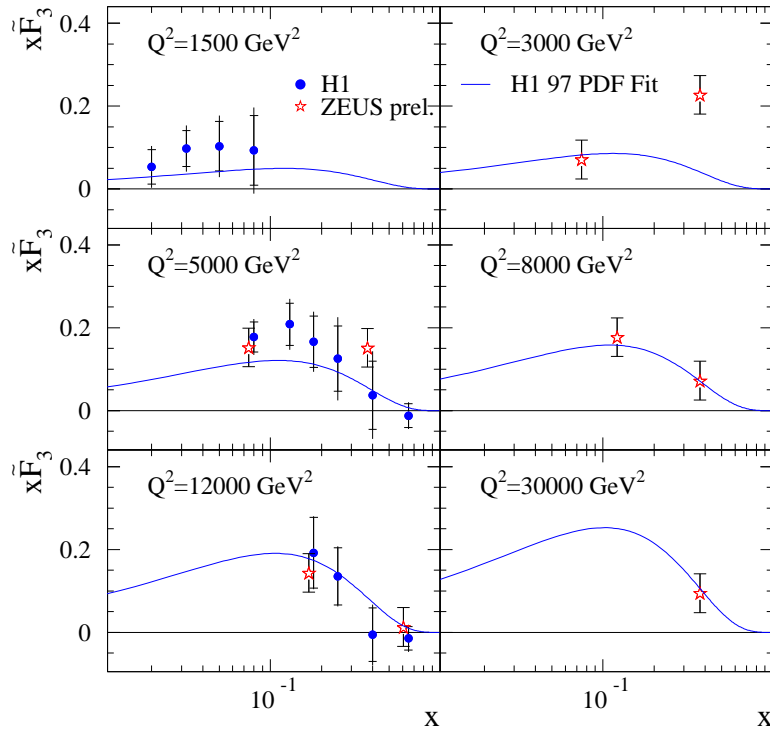


Fig. 13. The xF_3 structure function as determined by H1 and ZEUS as a function of x in six bins of Q^2 .

and 1.5 events, respectively. Unfortunately, this exciting observation is not confirmed by ZEUS, which, for the same cut in p_T^X , sees one event in each category compared to the Standard Model expectation of 1.1 and 1.3, respectively. Intensive discussions between the two experiments have not revealed any reason why H1 might artificially produce such an excess nor why ZEUS should not observe it. It would therefore seem that there must be an unlikely fluctuation: either the H1 observation is an upward fluctuation from the Standard Model, or ZEUS has suffered a downward fluctuation from a signal for new physics. More data from HERA II will be required to resolve this puzzle.

One possible source of an excess of events with isolated leptons with missing transverse momentum would be from a flavour-changing neutral current process producing single top quarks. Both H1 and ZEUS have used the samples described above to put limits on the FCNC couplings of the γ to light quark-top quark vertices. The results are shown in figure 16. Also shown are the limits from LEP and CDF, which are complementary to those from HERA, in the sense that, since the Z -exchange cross section at HERA is so much smaller than that for γ

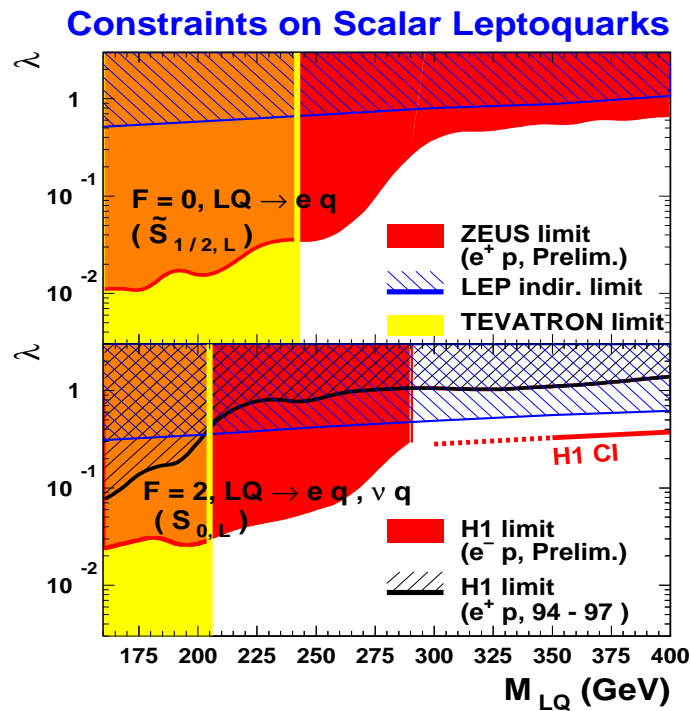


Fig. 14. Limits on coupling strength λ versus mass M_{LQ} for leptoquarks. The top plot shows limits for fermion number = 0 leptoquarks decaying into the eq final state from ZEUS. The lower plot shows limits from H1 for fermion number = 2 leptoquarks decaying into both eq and νq final states. Also shown are limits obtained from the Tevatron (yellow shaded area) and LEP (blue striped area). These leptoquark species have identical quantum numbers to squarks that violate R-parity.

exchange, the HERA data limit only the photon coupling.

3 HERA II physics

Many of the physics results discussed above, particularly those at high Q^2 , are statistics limited. Moreover, there is a natural build-up of transverse polarisation of the lepton beam in HERA that occurs through the Sokhlov-Ternov effect [16]. As very successfully demonstrated at HERMES using gas targets, this transverse polarisation can be rotated into the longitudinal direction and utilised to do physics. The installation of spin rotators in H1 and ZEUS would allow polarisation studies to be carried out at very much higher Q^2 . This is particularly interesting to study the chiral properties of the electroweak interaction.

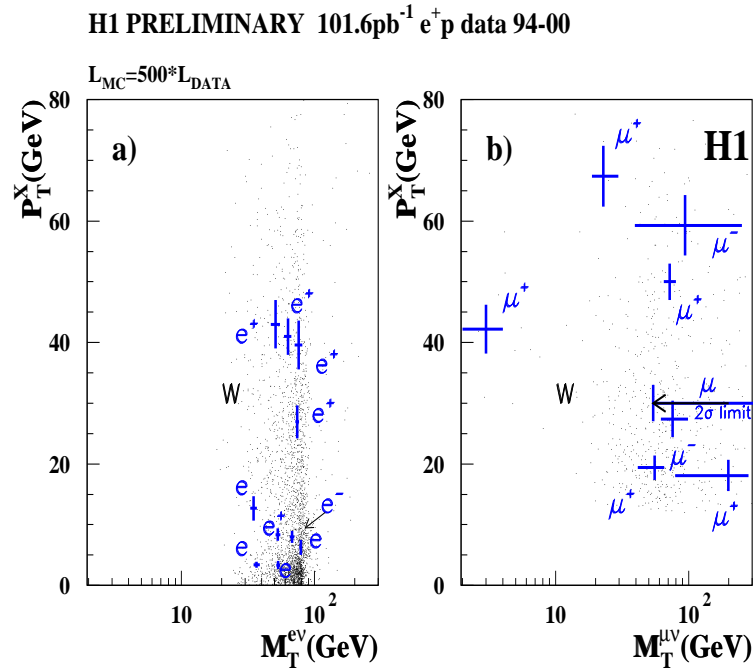


Fig. 15. Distribution of transverse mass versus the p_T of the hadronic system for H1 events containing a) isolated electrons and b) isolated muons. The dots show the distribution of Standard Model W Monte Carlo events corresponding to a luminosity 500 times that of the data.

For these and several other reasons, it was decided to embark on a major upgrade of both the HERA accelerator and the H1 and ZEUS detectors. The aim of the HERA II programme is to produce a factor of approximately five increase in luminosity and accumulate 1 fb^{-1} of data with both electron and positron collisions in both longitudinal polarisation states.

The changes to the HERA accelerator include the replacement of 480 meters of the vacuum system and the design and installation of almost 80 magnets in the region around the H1 and ZEUS interaction points. In particular, superconducting quadrupole focussing elements were inserted inside both detectors to reduce the beam emittance and spin rotators were installed on either side of the H1 and ZEUS interaction regions.

Both the ZEUS and H1 detectors have undergone a massive programme of consolidation and repair work, as well as major detector upgrades. In the time available I can only discuss briefly the changes made to ZEUS; the general thrust of the upgrade is similar in the two detectors, but the details are different.

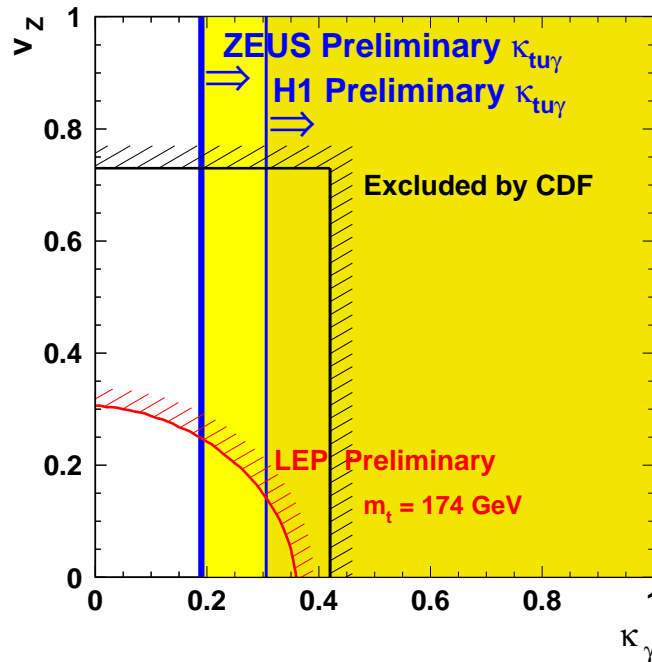


Fig. 16. Limits on flavour-changing neutral current coupling strength for single top production. Limits from H1 and ZEUS are plotted on the two-dimensional space of the photon and Z coupling strengths. Also shown are similar limits from the combined LEP experiments (to the right of the shaded curve) and from CDF (to the right of the black shaded lines).

3.1 Upgrades to ZEUS for HERA II

The ZEUS upgrades have concentrated in three main areas: the vertex region; the forward (= proton beam) direction; and the luminosity monitoring.

3.1.1 The vertex region The tagging of the large flux of heavy quarks (charm and beauty) produced at HERA II can be greatly enhanced by the installation of a high-precision charged-particle detector as close as possible to a thin beampipe. The ZEUS MVD [17, 18] consists of 20 μm pitch n -type silicon-strip detectors with p^+ -type implants. The readout pitch is 120 μm , leading to more than 200,000 readout channels, which are digitised by a custom-built clock, control and ADC system. The detectors are organised in two main groups: a “barrel”, which surrounds the elliptical 2 mm-thick ($\sim 1.1\%$ of a radiation length) aluminium-beryllium beam-pipe; and four “wheels”, consisting of wedge-shaped detectors mounted perpendicular to the beam-line in the forward direction from the interaction point. Figure 17 shows one half of the MVD before installation at DESY. In the barrel region, the ladders, each of which consists of five silicon

detectors, and halves of the four forward “wheels”, can be seen, as can the dense array of readout and services cables and the cooling system. The complete MVD was installed in ZEUS in April 2001 and has been fully integrated with the ZEUS DAQ system; both cosmic-ray and beam-related data have been taken.

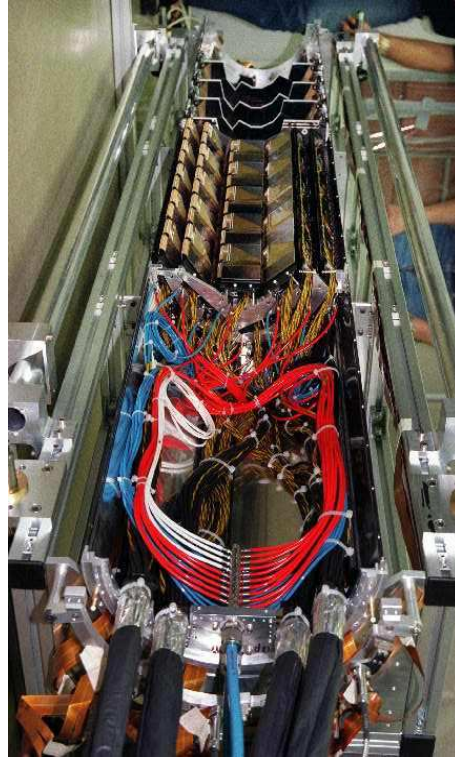


Fig. 17. A photograph of one half of the MVD, showing the barrel ladders, one half of each of the four forward wheels and the cables and services.

The physics programme addressed by the MVD is that of the flavour decomposition of the proton and photon and the search for physics beyond the Standard Model. The measurements of the semi-inclusive charm structure function, F_2^c , made by both experiments [19, 20] are shown in figure 18. The large increase in luminosity of HERA II, together with the ability to tag heavy-quark decays in the MVD, should greatly improve the measurement of F_2^c . After about 500 pb^{-1} , an uncertainty of around the 2% currently measured on F_2 should be obtained. In addition, b -quark production can be measured precisely; a Monte Carlo simulation [21] of a measurement of F_2^b/F_2^c after 500 pb^{-1} is shown in figure 19.

It should also be possible, from a combination of neutral and charged current measurements, to separate out the u, d, s, c, b and g contribution to F_2 .

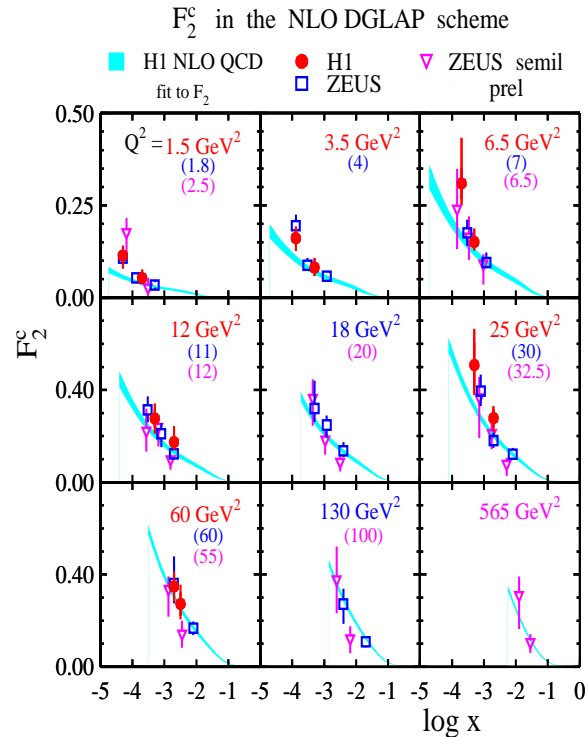


Fig. 18. Values of the charm structure function, F_2^c from the H1 and ZEUS experiments in bins of Q^2 as a function of $\ln x$. The shaded curves show the predictions from the NLO QCD fit to the inclusive F_2 data by H1.

3.1.2 Charged-particle tracking in the forward direction The higher luminosity expected at HERA II will increase the number of very high- Q^2 events in which the electron or positron is scattered into the forward direction. It will also give access to rare processes, including possible physics beyond the Standard Model, which tend to have forward jets and/or leptons. The pattern-recognition capabilities of the ZEUS Forward Tracker have therefore been improved by the replacement of two layers of transition-radiation detector by layers of straw tubes. The straws are approximately 7.5 mm in diameter and range in length from around 20 cm to just over 1 m. They are constructed from two layers of 50 μm kapton foil coated with a 0.2 μm layer of aluminium, surrounding a 50 μm wire at the centre. The straws are arranged in wedges consisting of three layers rotated with respect to each other to give three-dimensional reconstruction. Each of the two “supermodules” consists of four layers of such wedges.

3.1.3 Luminosity monitor The measurement of luminosity at HERA II must cope with the greatly increased synchrotron-radiation background and the higher probability for multiple bremsstrahlung photons in one beam crossing. To

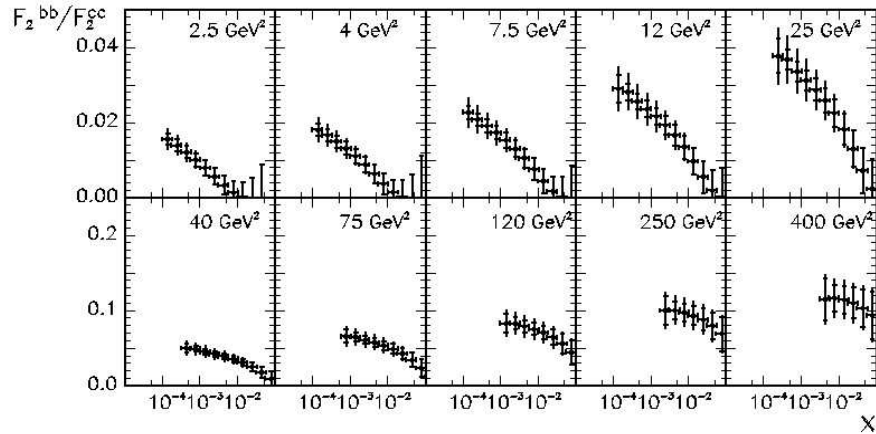


Fig. 19. The MC prediction for the ratio of the contribution to F_2 of b -quark to c -quark production in Q^2 bins as a function of x after 500 pb^{-1} of data at HERA II.

compensate for this, two devices, with very different systematic uncertainties, have been constructed. Both devices use the information from a small calorimeter placed around 6 m from the interaction point which detects the radiating electron.

The photon calorimeter is a lead-scintillator sandwich with a position detector consisting of strips of scintillator. In order to cope with the synchrotron radiation background, an “active filter”, consisting of two carbon absorbers, each of two radiation lengths, alternating with Aerogel Cerenkov detectors has been constructed. The absorbers protect the calorimeter from radiation damage, while the Cerenkov detectors detect high-energy photons that convert in the absorbers, allowing the calorimeter energy to be corrected and good resolution to be recovered.

The pair spectrometer is situated downstream of an exit window corresponding to around 12% of a radiation length. The electron-positron pairs that convert therein are separated by a dipole magnet and detected in a pair of tungsten-scintillator sandwich calorimeters.

The “6 m tagger” consists of a $10 \times 10 \times 5$ cm tungsten-scintillating fibre calorimeter next to the beam-pipe and situated inside one of the HERA magnets.

Each of these devices uses a newly developed common electronic readout system. With the exception of the tagger, which will be installed in January 2002, all these devices have been installed and been readout. The calorimeter is reporting luminosity values online to the accelerator physicists while the spectrometer is currently being commissioned. It is hoped that the reduction of systematic error that can be obtained from independent luminosity measurements using very different techniques will allow a precision of around 1% to be attained.

3.2 Polarisation

Polarisations of around 65% have been achieved at HERA I. It is hoped to increase the accuracy with which the polarisation can be measured to $\delta P/P \sim 2\%$ per bunch per minute. This will be achieved by a collaboration between H1, HERMES, ZEUS and the HERA machine in the POL2000 project. The collaboration has constructed two instruments, one to measure the longitudinal polarisation and the other to measure the transverse polarisation. Both detect asymmetries in back-scattered light from high-intensity polarised lasers.

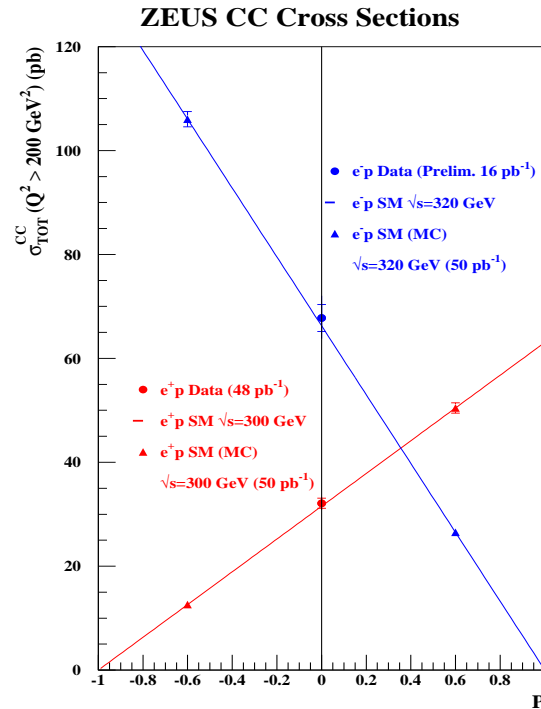


Fig. 20. The cross section for charged current interactions. The points at $P=0$ are obtained from ZEUS preliminary results at the indicated centre-of-mass energies, while those at non-zero polarisation are Monte Carlo simulations of the expected accuracy in ZEUS assuming the Standard Model cross section for an integrated luminosity of 50 pb⁻¹ per point.

The combination of high-precision measurements of both luminosity and polarisation will be important in a wide range of HERA II physics, particularly in the electroweak sector. The charged current cross section should vanish for the appropriate combinations of lepton charge and polarisation. A measurement at three polarisations, such as shown in figure 20, even with an integrated luminosity of only 50 pb⁻¹ per point, will provide an accurate test of this prediction and thereby give sensitivity to possible new currents outside the Standard Model.

Strong polarisation effects are also predicted at high Q^2 in neutral current interactions, where, e.g. at $Q^2 = 10^4 \text{ GeV}^2$ and $x = 0.2$, there is a factor of two difference between the predicted cross sections for left- and right-handed electrons.

In addition to the use of precise luminosity and polarisation information in the study of electroweak processes, polarisation also offers an invaluable tool in the study of possible signals beyond the Standard Model. Varying the polarisation to reduce the cross sections of Standard Model processes can improve the signal to background for new physics signals, such as leptoquarks or supersymmetric particles that violate R parity, for which HERA will be competitive with the Tevatron for the next few years.

4 The relevance of HERA physics to LHC experimentation

At an LHC Symposium, it is relevant to comment on the importance of HERA physics to experimentation at LHC. The HERA I programme has added enormously to our understanding of the strong interaction, in both the “hard” and “soft” regimes, and HERA II promises similar progress in the space-like electroweak interaction and in the search for physics beyond the Standard Model. The distributions of partons inside the proton which are being accurately measured at HERA are precisely those that collide at LHC. In addition to these obvious generic links between HERA and LHC physics, there are some very specific areas where information from HERA impinges directly and importantly on LHC physics. The two most important, and which are therefore discussed here, are the determination of luminosity and the search for new physics processes at LHC.

4.1 Luminosity determination at LHC

Much of the most exciting physics at LHC does not require an accurate luminosity measurement; for example, the Higgs can be discovered without any knowledge of the luminosity. However, any cross-section measurement, the absolute determination of branching ratios and many precision measurements do require such knowledge. The accuracy required is relatively modest, around 5% [22]. However, the task of making a luminosity determination to even this accuracy is very challenging.

There are three main ways that have been discussed to determine the luminosity [23]:

1. measure the total and elastic cross sections;
2. measure QED lepton-pair production
3. measure inclusive W and/or Z production

Since the second method is independent of HERA information, it is not discussed further.

The total and elastic cross sections are dominated by soft processes and can be well explained by Regge Theory and the Pomeron. The Optical Theorem links the elastic and total cross sections via

$$\left. \frac{d\sigma_{el}}{dt} \right|_{t=0} = \sigma_{tot}^2 \frac{(1 + \rho^2)}{16\pi}, \quad (11)$$

where ρ is the ratio of the real to imaginary parts of the forward elastic amplitude. If both the elastic and total rates can be measured then the luminosity can be inferred, since the elastic rate is proportional to $\sigma_{tot}^2 \cdot \mathcal{L}$ while the total rate is proportional to $\sigma_{tot} \cdot \mathcal{L}$. Unfortunately, it is very difficult to measure at $t = 0$ at LHC! A model that permits an extrapolation from the smallest accessible t ($\sim 0.01 \text{ GeV}^2$) to $t = 0$ is required. Such models exist [24], but are crucially dependent on detailed properties of the soft Pomeron and of diffraction and elastic scattering in general that are under intensive investigation at HERA.

Another problem with the first method is that the measurement of elastic scattering is really limited to relatively low luminosities. In order to cope with the very high luminosities required at LHC it is necessary to use another method, which can be cross-calibrated with the first method at low luminosities and then take over. An attractive possibility is the third method, measuring W and Z production rates. Although the rate at the highest LHC luminosities compares favourably with that of Bhabha scattering used at LEP, it suffers from the disadvantage that our ability to calculate the QCD processes which produce vector bosons is significantly inferior to the QED or Electroweak theories used for Bhabha scattering. Nevertheless, NNLO QCD predictions are available with an estimated accuracy of $\sim 1\%$, much better than the required accuracy. The accuracy is more likely to be limited by our knowledge of the strong coupling constant, α_s , whose value is unlikely to be known to comparable precision before LHC operation. Further requirements are that the densities of the partons that collide to produce the vector bosons should be accurately known at the appropriate values of x . In the LHC central detectors, this corresponds to approximately $10^{-4} \leq x \leq 10^{-1}$, a range well within the ability of HERA to determine with the requisite errors before LHC begins operation. It transpires that the errors on the quark densities are currently the dominant ones. The final ingredient necessary to use W and Z production reliably as a luminosity monitor is the ability to extrapolate with confidence from the Q^2 range at which the parton distribution functions are measured at HERA to the much higher values relevant at LHC. The adequacy of the standard DGLAP evolution has now been established at HERA for the kinematic range relevant to boson production in the central rapidity region at LHC. However, it is as well to remember that there will certainly be regions of phase space accessible to careful experimentation at LHC where deviations from DGLAP would be expected and should be observable [25].

4.2 Searches for new physics at LHC

The enormous factor by which background processes exceed interesting events is the dominant consideration in experimentation at LHC and the one that sets the performance requirements for much of the apparatus, in particular the trigger.

It is clear, therefore, that a detailed understanding of the backgrounds, which, in contrast to previous experiments, come from beam-beam collisions rather than single-beam interactions, is vital. Essentially all of the background originates from QCD parton-parton interactions and is therefore once again governed by the parton distribution functions determined largely by HERA data.

In addition to the necessity to understand the backgrounds, some of the processes studied at HERA can also give rise to interesting signals for new physics. In general, many of the possible new species of particles expected within the discovery potential of LHC would be colourless and therefore their production might well be associated with rapidity gaps. An important example of such a process is diffractive production of the Higgs. Since from Tevatron data it can be predicted that Standard Model production of events with large rapidity gaps is down by about two orders of magnitude compared to normal events, a large improvement in signal to noise could be obtained provided that the diffractive Higgs production is not similarly suppressed. Unfortunately there are several models [24], whose predictions for the ratio between diffractive Higgs production and the dominant $gg \rightarrow H^0$ range between 10^{-1} and 10^{-12} . The spread between these models is predominantly due to the extent to which the production is dominated by a “soft” or a “hard” Pomeron. The elucidation of the properties of such Pomerons is currently a subject of intensive study at HERA. The other major factor that effects the possibility of observing the Higgs via diffractive production is the extent to which the rapidity gaps thus produced are “filled in” by other processes such as minimum-bias interactions from the overlapping protons, bremsstrahlung from the partons participating in the hard collision and radiation from the partonic constituents of the Pomeron itself. The well-known discrepancy between the CDF rapidity-gap data and the prediction from the rate of such events at HERA assuming simple vertex factorisation gives a good handle with which to estimate the size of such effects [26].

5 Future prospects for lepton-proton physics

The future for lepton-proton physics is at least clear for the period up until around 2006, during which the upgraded HERA II accelerator has an exciting physics programme, as discussed in section 3. For the period beyond that, there are several possibilities.

There are already intensive discussions on a programme at HERA beyond that of HERA II, unsurprisingly labelled HERA III. The programme could include lepton-deuteron scattering, with both polarised and unpolarised deuterons, polarised electron-polarised proton scattering, electron-nucleus scattering, dedicated experiments on low x physics and diffraction as well as a continuation of the HERMES programme of polarised electron on gas target scattering. The dynamic of this programme is driven mostly by unanswered questions in low- x physics, particularly questions such as saturation, as discussed in section 2.1, which probably cannot be solved with HERA I data and cannot be addressed at HERA II, since the relevant kinematic region is shadowed by the superconducting quadrupoles installed inside H1 and ZEUS. The eN option would be particularly suited to address these questions, since there are good theoretical

grounds to believe that the density of quarks in such collisions can be substantially increased over what is possible in ep collisions. Another incentive is the desire to enter completely unexplored kinematic regions of spin physics. It seems likely that an exciting physics programme can be constructed. However, the possibility of its implementation is closely coupled to the TESLA project, which is clearly the first priority of the DESY laboratory. Several aspects of the HERA III programme, in particular the polarised-proton option, would require substantial investment of both money and accelerator physicists, which currently seems unlikely to be available inside the laboratory without substantial external funds becoming available.

A rather similar set of physics objectives can be addressed with the Electron-Ion Collider (EIC) project at RHIC at Brookhaven. Polarised protons are readily available; the parameters being discussed would produce ep collisions at $\sqrt{s} \sim 100$ GeV with a luminosity around $5 \cdot 10^{32} \text{ cm}^{-2} \text{ s}^{-1}$ and eA collisions at $\sqrt{s} \sim 65$ GeV with luminosity around $6 \cdot 10^{30} \text{ cm}^{-2} \text{ s}^{-1}$. The advantages of this proposal with respect to HERA III are the easy availability of polarised protons from currently available infrastructure, acceleration of heavy nuclei up to gold and the higher luminosity. The disadvantages are that it is relatively expensive to build the new electron storage ring and that the centre-of-mass energy available is considerably lower than at HERA. Once again, extensive discussions and workshops are underway both in the particle physics and nuclear physics communities to discuss this project.

In the more distant future, further exciting options open up. The neutrino factory concept would provide enormous fluxes of neutrinos (approximately four orders of magnitude above what can be achieved with conventional sources) which would enable a rich programme of fixed-target neutrino physics including for the first time the possibility of using polarised targets.

Another possibility is to construct ep colliders with higher energy than HERA. The THERA proposal would utilise the electrons from the TESLA superconducting linac to collide with protons in the HERA ring. By using the full length of the linac, electrons of up to 500 GeV could be collided, producing a centre-of-mass energy of 1.35 TeV. Such a machine would extend the HERA kinematic range by two orders of magnitude in Q^2 and one in x . Exploration of the x range around 10^{-6} with Q^2 well into the perturbative QCD regime would become possible, allowing a comprehensive investigation of all the problems in low- x physics, saturation and diffraction discussed above. It would also be an ideal machine to measure parameters of any possible new state with leptoquark-like properties, such as many states in R-parity-violating supersymmetry. THERA also has discovery potential for certain classes of possible new states, for example right-handed or excited neutrinos.

The major limitation with THERA is the attainable luminosity, which is limited by colliding electron bunches from the linac rather than in a storage ring. It may be possible to get up to $10^{31} \text{ cm}^{-2} \text{ s}^{-1}$, but it will not be easy, and $10^{30} \text{ cm}^{-2} \text{ s}^{-1}$ would be a more conservative value. This will certainly be adequate for the low- x physics, but will limit studies at the highest Q^2 . Such a luminosity limitation is avoided in the “LHC \times LEP” machine, in which new magnets could be built to reinstate the LEP ring and the electrons collided

with protons in LHC. Although this option has been left open at CERN, at the moment it is not being actively pursued.

6 Summary

In the last decade, HERA I has changed our perception of QCD out of all recognition. In many cases the precision of the data mandate NNL, or even high order, QCD predictions. The study of diffraction and the transition region between soft and hard physics may be beginning the era of quantitative study of the central problem of the strong interaction, confinement.

The precision attained on the parton distribution functions in the proton, mostly with HERA data, will directly influence many of the physics topics at LHC. In addition, some of the processes studied at HERA may well lead to distinctive signatures for new physics and contribute to the luminosity determination necessary for many precision studies.

Now that the first collisions have been achieved in HERA II with specific luminosities close to the design, the immediate future for ep physics seems bright. Ideas for further developments such as HERA III and EIC are already gathering momentum, and possibilities for the distant future are also in place. These latter will surely be thrown into a much clearer light by what we all hope and expect to be revolutionary discoveries at LHC. In any case, ep physics has had a glorious past and I am confident will continue to produce much excitement in the future.

Acknowledgements

I am grateful to Gino Saitta and his colleagues from INFN Cagliari and Roma for organising a splendid workshop in beautiful surroundings. I thank Carlo Bosio for his patience with numerous deadline postponements for this manuscript. I am grateful to Masahiro Kuze for a careful reading of the manuscript; as usual, he improved both my physics and my grammar.

References

1. E. Rutherford, *Phil. Mag.* **21** (1911) 669
2. H. Geiger and E. Marsden, *Proc. Roy. Soc. Lond.* **82** (1909) 495
3. see J.I. Friedman and H.W. Kendall, *Ann. Rev. Nucl. Science* **22** (1972) 203
4. H1 Collaboration, C. Adloff et al., *Eur. Phys. J.* **C13** (2000) 609
5. H1 Collaboration, C. Adloff et al., *Eur. Phys. J.* **C21** (2001) 33
6. ZEUS Collaboration, S. Chekanov et al., *Eur. Phys. J.* **C21** (2001) 443
7. ZEUS Collaboration, J. Breitweg et al., *Phys. Lett.* **B481** (2000) 213
8. L.N. Lipatov, *Sov. J. Nucl. Phys.* **20** (1975) 95
9. V.N. Gribov and L.N. Lipatov, *Sov. J. Nucl. Phys.* **15** (1972) 438
10. G. Altarelli and G. Parisi, *Nucl. Phys.* **B 126** (1977) 298
11. Yu.L. Dokshitzer, *Sov. Phys. JETP* **46** (1977) 641
12. B. Foster, *Phil. Trans. R. Soc. Lond.* **A359** (2001) 325, and references therein
13. K. Golec-Biernat and M. Wüsthoff, *Phys. Rev.* **D59** (1999) 014017

14. K. Golec-Biernat and M. Wüsthoff, Phys. Rev. **D60** (1999) 114023
15. H1 Collaboration, C. Adloff et al., Eur. Phys. J. **C19** (2001) 269
16. A.A. Sokholov and M. Ternov,
Sov. Phys. Dokl. **8** (1964) 1203
17. A. Garfagnini, Nucl. Instr. and Meth. **A435** (1999) 34
18. E. Koffeman,
Nucl. Instr. and Meth. **A473** (2001) 26
19. ZEUS Collaboration, J. Breitweg et al., Eur. Phys. J. **C12** (2000) 35
20. H1 Collaboration, C. Adloff et al., hep/ex 0108039, to be published in Phys. Lett.
21. K. Daum et al., in Proceedings of the Workshop on Future Physics at HERA, ed.
A. De Roeck, G. Ingleman and R. Klanner, Vol. 1, p. 89, DESY, Hamburg, (1996).
22. A. Martin, hep/ph 0103296
23. see various articles in Proceedings of the First Workshop on Forward Physics and
Luminosity Determination at the LHC, Helsinki, (2000)
24. V.A. Khoze, hep/ph 0105224, and references therein
25. J. Stirling, talk given at First Workshop on Forward Physics and Luminosity De-
termination at the LHC, Helsinki, (2000)
26. A.B. Kaidalov et al., Eur. Phys. J. **C21** (2001) 521